Controlled gene delivery using Layered double hydroxides for cancer treatment

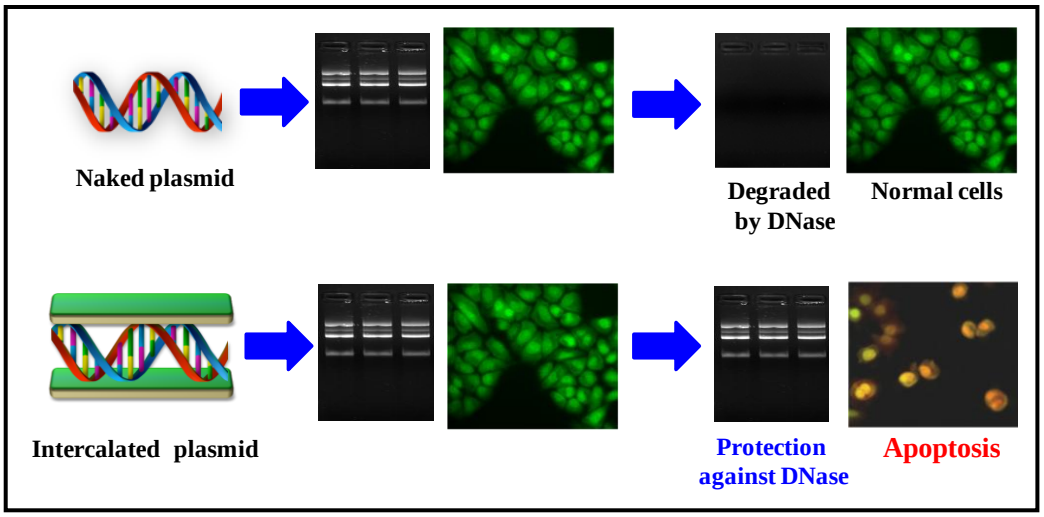

This chapter describes development of Li-Al based LDHs that can protect plasmid vector from outside environments and efficiently deliver it into mammalian cancer cell inducing apoptosis.

5.1 Introduction

Gene therapy is considered to be an efficient therapeutic technique for the treatment of genetic diseases such as cancer [Cross et al., 2006; Zhang et al., 2016], hepatitis [Yang et al., 2010], and sickle-cell anemia [Olowoyeye et al., 2014]. However, the cellular membrane is one of the major obstacles for the efficient delivery of naked nucleic acids into the cells since it allows only selective entry by passive or active transport mechanisms. Therefore, gene therapy necessitates efficient delivery of such molecules to cells because naked nucleic acids alone are unable to get across cell membranes. Gene delivery carriers are broadly divided into two categories; viral and nonviral systems. Although the viral systems are the most effective but arise safety issues such as immunogenicity and the possibility of gene recombination. Among the nonviral vehicles, cationic polymer based systems have shown tremendous potential due to having unique properties such as degradability, reproducibility, ability to deliver higher molecular weight genes, low cost, ease of modifications and high transfection efficiency. However, to enhance transfection efficiency, these polymeric vehicles surface are often coated with positive moieties such as poly(-L-lysine) (PLL) and polyethylenimine (PEI) which are cytotxic in nature.

Inorganic nanocarriers possess several advantages over polymeric ones for gene delivery system such as relatively low toxicity, better transfection efficiency, better protection against outer environments, better endosomal escape and easy surface modification. Among the inorganic nanocarriers mesoporous silica [Radu et al., 2004], gold [Pissuwan et al., 2011], quantum dot [Yezhelyev et al., 2008], carbon nanotubes [Bates et al., 2013], and layered double hydroxide nanoparticles [Xu et al., 2007] are the prominent ones used for gene delivery. Nucleic acids that are simply conjugated or adsorbed onto the surface of nanoparticle can be easily degraded by nucleases. Therefore, it is desired to protect

this gene into a suitable space for protection from degradation until they reach active site where they should be released. Among various inorganic nanoparticles, layered double hydroxides (LDHs) is emerged as a promising delivery vehicles because it has such advantages as anion exchange capacity, easy surface manipulation, excellent biocompatibility, long-term stability, and low cost. The unique anion exchange performance of LDHs meets the requirement of encapsulating bioactive molecules with negative charge in physiological media. Such bioactive molecules can be intercalated between the gallery of hydroxide layers by a facile anion-exchange. The negatively charged bioactive molecules intercalated into the interlayer gallery spaces would gain extra stabilization energy due to the electrostatic interaction between cationic LDHs host layers and anionic biomolecules. Moreover, the hydroxide layers can play the role of a reservoir to protect intercalated DNA from DNase degradation. Again, the electrostatic repulsive interaction between negatively charged cell membranes and anionic DNA molecules during the uptake process can be easily overcome through hybridization between LDH and DNA. This chapter deals with the development of Li-Al based LDHs system as a gene delivery carrier for the application of cancer treatment.

5.2 Results and Discussion

5.2.1 Synthesis of Li-Al LDH nanoparticles

The bright field TEM images LDHs particles exhibit discrete hexagonal disc-like shaped particles with lateral dimension of ~85±3 nm while predominantly stacking of disc-like shaped particles and some agglomerated morphology have been observed in the corresponding DNA intercalated LDH (LDH-DNA) having the lateral dimension of 91±4 nm (**Figure 5.1a**). The surface morphology through HRSEM of LDH and LDH–DNA is shown in **Figure 5.1b**. Similar to TEM images, HRSEM also reveals disc-like morphology of LDHs with dimension 87±2 nm, and after the intercalation of DNA in

LDH–DNA disc-like structure of size 93±3 nm are noticed. **Figure 5.1c** demonstrates the AFM images of the dried suspension indicating well dispersed particle with size 92 and 96 nm for LDH and LDH-DNA respectively. Dynamic light scattering study reveals that LDH and LDH-DNA have particle dimensions of 125±2 and 137±3 nm respectively.

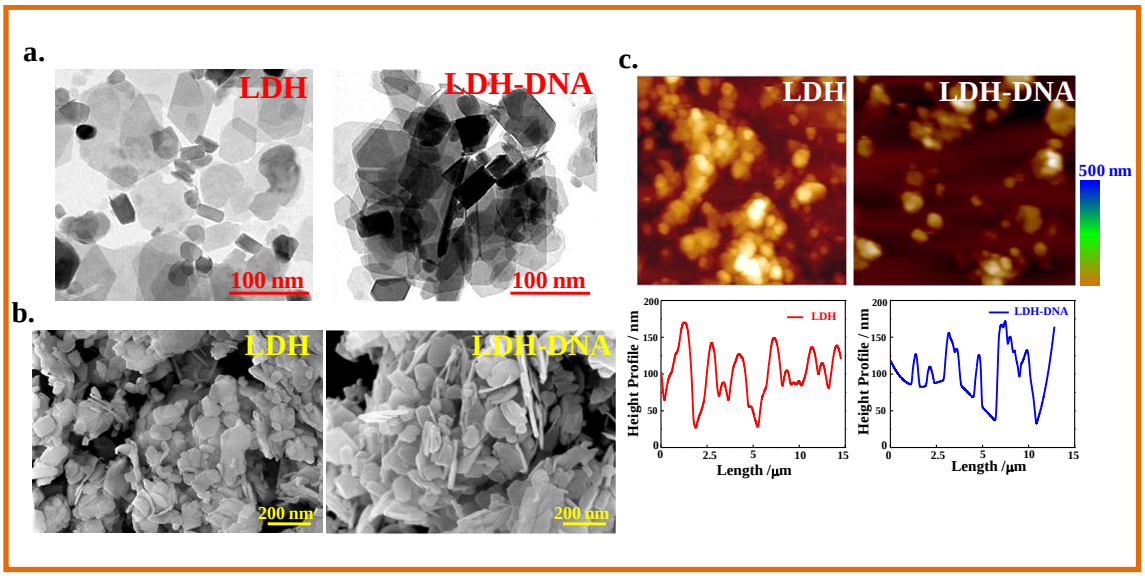

Figure 5.1: (a) Bright field TEM images of pristine LDH and DNA intercalated LDH (LDH-DNA); **(b)** HRSEM micrographs of LDH and LDH-DNA, and, **(c)** AFM topographs of LDH and LDH-DNA with height profile.

5.2.2 Effect of DNA intercalation on structure and physicochemical properties

Figure 5.2a shows the X-ray diffraction patterns of the LDH–DNA nanohybrids compared to that of the corresponding parent pristine LDH. The reflection from (003) crystallographic plane represents the thickness of the hydroxide layer plus the interlayer spacing. The diffraction peaks appear from (003), (006) and (009) crystal planes, as well as two well separated arising from (110) and (113) basal planes, indicate the formation of well-crystallized and well-ordered layer structure in pristine LDH. The intercalation of DNA molecules into the LDH interlayer gallery is clearly evidenced by the net increase

of the interlayer distance, from 0.76 nm for pristine LDH to 2.14 nm for DNA complex with LDH (LDH–DNA).

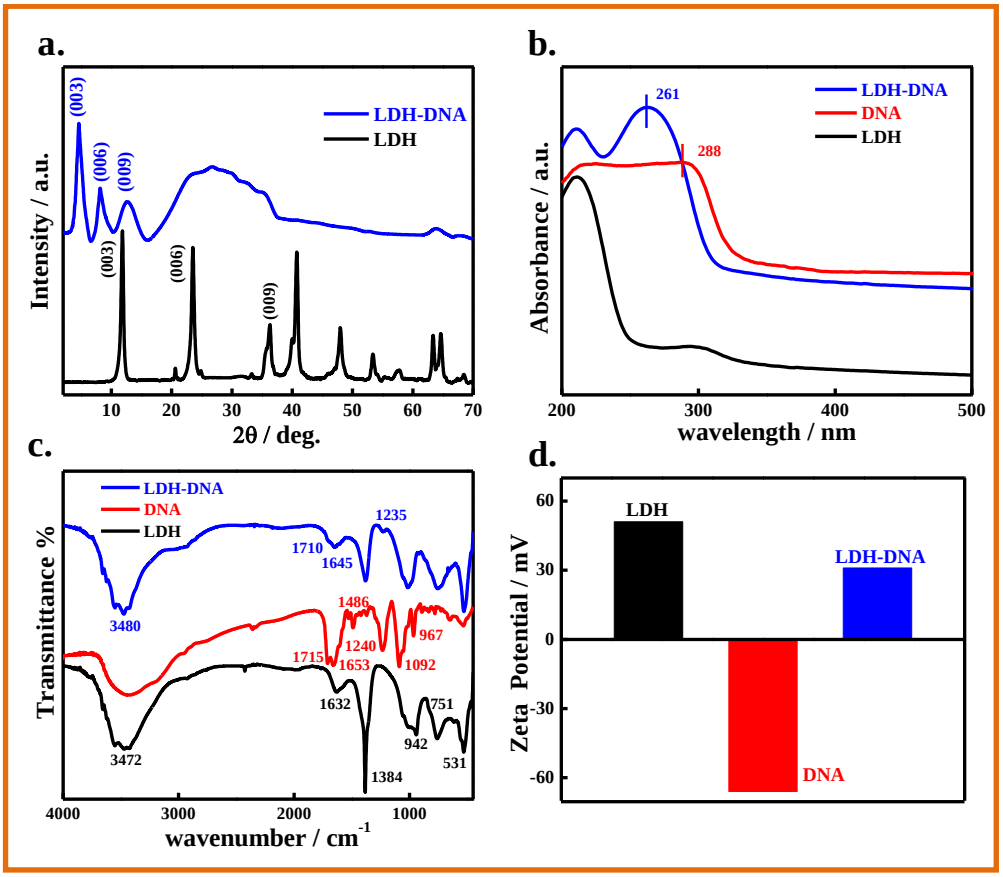

Figure 5.2: (a) Powder X-ray diffraction patterns in the 2θ range of 2–70^{o} of LDH and LDH–DNA nanohybrid; **(b)** Solid state UV-Vis spectra of pristine LDH, naked DNA and LDH–DNA nanohybrid; **(c)** FTIR spectra of the indicated samples, and, **(d)** Zeta potential analysis of the samples.

The comparative solid state UV–Vis spectra of pristine LDH, naked DNA and LDH–DNA nanohybrid are shown in **Figure 5.2b**. The absorption spectrum of naked DNA exhibits peaks at 288 nm. After intercalation, a blue shifting to 261 nm of this peak is observed in LDH–DNA due to the electrostatic interaction between the negatively charged DNA molecules and positively charged LDH host layers.

Intercalation of the DNA molecules into the LDH interlayer space is also confirmed by comparing the FTIR spectra for DNA intercalated LDH with pristine LDH and naked DNA **(Figure 5.2c)**. The spectrum of pristine LDH exhibits the intense broadband around 3470 cm^{-1} corresponding to the stretching vibration of the hydroxyl groups of LDH hydroxide layers and interlayer water molecules. The peak appears at ~1630 cm^{-1} is responsible for bending vibration of water molecules present in the interlayer gallery [Wang et al., 2007]. Again, the sharp band appears at 1384 cm^{-1} is assigned to the v_3 stretching vibration of interlayer NO_3^- [Chao et al., 2008]. In the energy region, the bands at 942, 751, and 532 cm^{-1} are attributed to M–O and M–O–H stretching vibrations in the brucite-like host layers of the LDHs. In the spectrum of naked DNA, the band at 1715 cm^{-1} is attributed mainly to guanine (G) C≡N stretching vibrations while the band at 1661 cm^{-1} is mainly associated with C=O stretching vibrations caused by thymine (T). Again, the band at 1610 cm^{-1} is assigned to adenine (A) base vibrations while the band at 1493 cm^{-1} is due to cytosine (C) vibrations. The bands appear at 1240, 1092 and 967 cm^{-1} attributes to the phosphate groups present in the DNA structure. After the DNA intercalation, LDH–DNA shows diluted (low intense) characteristic peak of nitrate group at 1384 cm^{-1} confirming the exchange of nitrates ions with the negatively charged DNA molecules and the other prominent characteristics DNA peaks.

The zeta potential measurement reveals that naked DNA molecules high negative surface charges (−66±3 mV), while pristine LDH exhibits high positive zeta potential value (51±3 mV) **(Figure 5.2d)**. The surface charge of DNA has been regulated after intercalation into LDH (31±2 mV), and this modified surface charge is expected to enhance internalization of LDH–DNA nanohybrids into cells.

5.2.3 Protection of DNA

For an efficient gene delivery, it is desirable that the DNA loaded complex should have the potency to protect the bound DNA against the external environmental conditions such as degradation by nucleases or heat induced damage. To evaluate the ability of the developed nanohybrids to provide protection to the intercalated DNA against nucleases present in the environment, DNase I protection assay is performed after incubating the LDH-pDNA complex in DNase I for different time intervals (2, 5, 10, 20, 60 and 120 min). After DNase I treatment, the complex pDNA was released from the LDH-pDNA nanohybrid after incubation at pH 2 before running on gel electrophoresis). **Figure 5.3a** shows that without DNase I treatment, pDNA complexed with LDH is almost completely released after the acid treatment. This observation clearly indicates LDH forms very stable complex with pDNA. After the DNase I treatment, naked pDNA (0.25 μg) is completely degraded within 20 min and hence is not detected on the gel. In contrast, the degradation of pDNA proceeds in much slower rate when intercalated with LDH. The quantitative determination is performed by densitometrically and is presented in **Figure 5.3b**. It is found that LDH effectively protects the complexed pDNA and ~93% DNA was found to be recovered after 20 min, 88 % after 1 h and ~80 % after 2 h while naked pDNA is digested within 20 min of exposure. These results therefore show the potential of LDH to provide protection to nucleic acids from degradation by nucleases.

To examine the ability of the developed nanohybrids to provide protection to the intercalated DNA against thermal damage, DSC analysis is performed. **Figure 5.3c** shows the DSC thermograms of naked DNA and LDH–DNA nanohybrid. The naked DNA exhibits a broad endothermic peak in the temperature range 65-80 ^{o}C which indicates it's melting [Duguid et al., 1996].The broadening of melting transition is attributed to the heterogeneous base composition present in the DNA structure. After

intercalation of the DNA between the LDH interlayer galleries, LDH protects it from its melting in this temperature region and increases its melting temperature to 145 ^{o}C. Again, the heat of fusion, ΔH associated with the melting of DNA reduces to 72 from its original value 118 64 J.g^{-1} for naked DNA. Hence, these results show the potential of LDH to provide protection to nucleic acids from thermal damage.

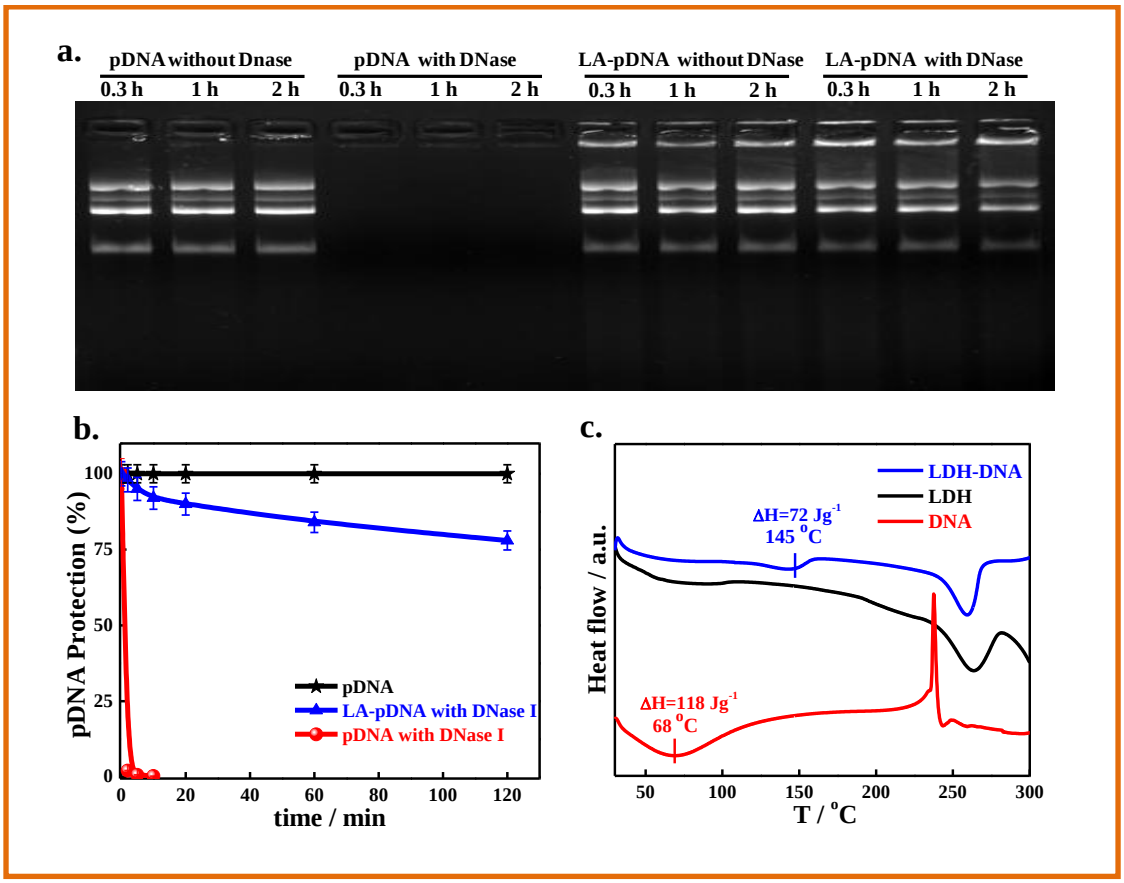

Figure 5.3: (a) DNase I protection assay; LDH-pDNA complex and naked pDNA were treated with DNase I for different time intervals. The complexed pDNA was released from the LDH-pDNA nanohybrid after incubation at pH 2; **(b)** The amount of DNA protected (%) after DNase I treatment was calculated as the relative integrated densitometry values (IDV), quantified, and normalized by that of pDNA values (without DNase I treatment) using Gel Documentation system (Syngene, U.K.), and, **(c)** Protection against thermal damage; DSC thermogram exhibiting that LDH interlayer gallery space can be used to protect the naked DNA from any thermal damage.

5.2.4 *In vitro* controlled release of DNA

In vitro release kinetics of DNA from LDH–DNA nanohybrid has been studied through UV-Vis absorption spectroscopy. **Figure 5.4a** demonstrates the cumulative percentage release of DNA in PBS media (pH ~ 7.4) at 37 ^{o}C. LDH–DNA nanohybrid exhibits an initial burst release that accounted for the ~ 55% DNA released in first 12 h, which is good for the priming of a therapeutic response. After the initial fast release profile, it follows a slow release kinetics pursuing a biphasic elution profile and continues to release for 42 h. The DNA molecules released from this nanohybrid through ion-exchange of these negatively charged DNA molecules by phosphate ions present in PBS medium. To understand release kinetics of DNA molecules from the nanohybrid in better way, a number of kinetic models such as Zero-order, first-order, Korsmeyer–Peppas and modified-Freundlich kinetic models have been exploited. The linear correlation coefficient (r^2) and other fitting parameter values obtained from the linear fittings of the DNA release data are presented in **Table 5.1**. Among these mathematical models, zero-order, first-order and Korsmeyer–Peppas give poor r^2 values ranging from 0.724 to 0.916 and are found not suitable to explain release behavior while the modified-Freundlich is found to be the most appropriate model for describing the mechanism of DNA release LDH–DNA nanohybrid (**Figure 5.4b**). Again, **Figure 5.4c** schematically demonstrates the ion exchange mechanism through which the DNA molecules released from the LDH interlayer gallery.

Table 5.1 Rate constants, linear correlation coefficients (r^2) and diffusion release exponent (n) obtained by fitting the DNAelease data from LA-DNA.

Sample	Zero-order		First-order		modified Freundlich		Korsmeyer-Peppas	
	k_0	r^2	k_1	r^2	k_M	r^2	n	r^2
LA–DNA	38.5±3	0.902	1.75±0.32	0.821	0.47±0.22	0.992	0.65±0.14	0.922

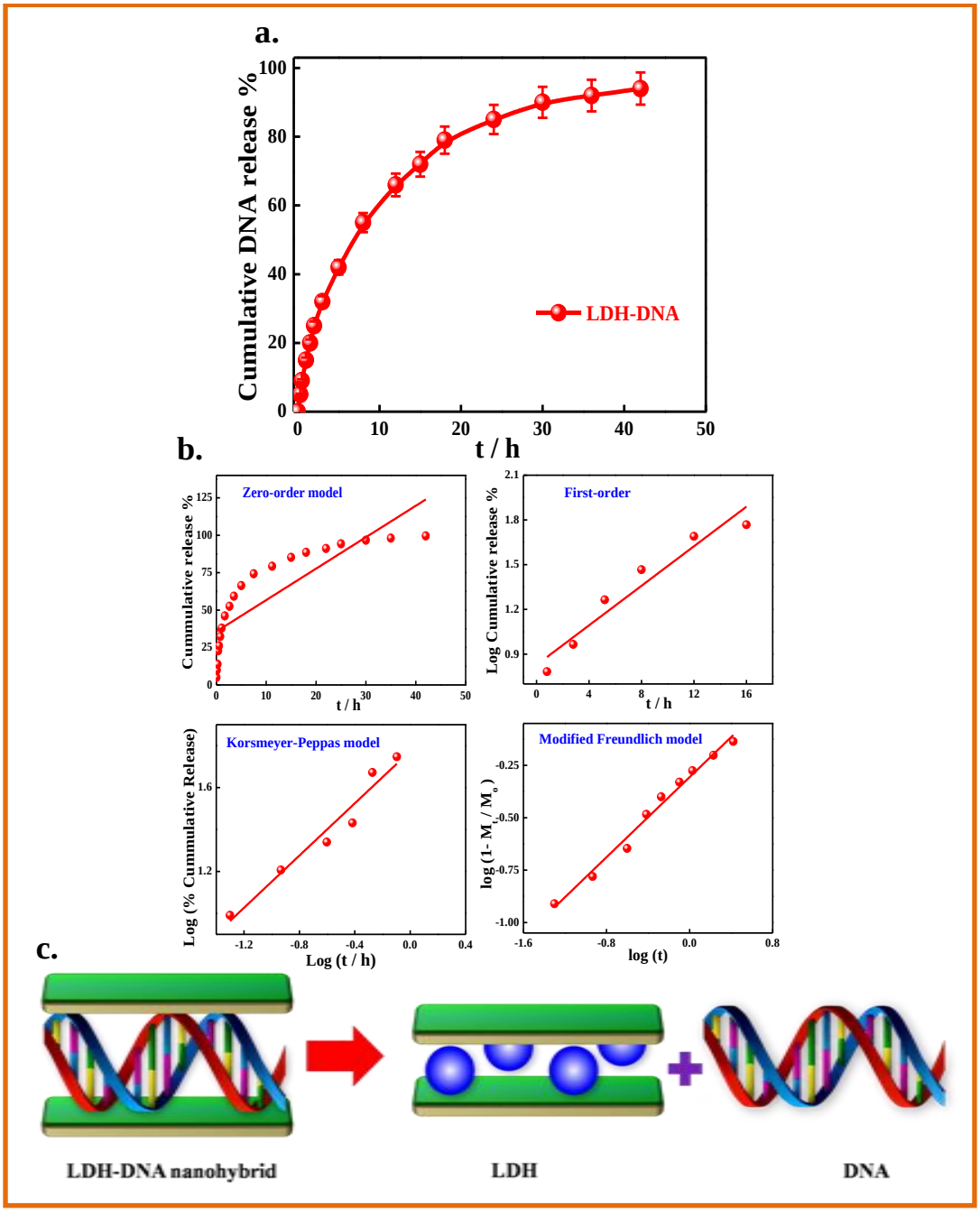

Figure 5.4: *In vitro* controlled release experiment and its mechanism; **(a)** Cumulative percentage DNA release profile from LDH-DNA nanohybrid in PBS at pH ~7.4 at 37 °C. The data points are plotted as mean ± SD values obtained from three different set of experiments; **(b)** Linear fitting of the DNA release data to zero order, first-order, Korsmeyer–Peppas and modified Freundlich model; **(c)** Schematic representation of possible DNA release mechanisms from LDH-DNA nanohybrid.

5.2.5 *In vitro* cytotoxicity

Cell adhesion is an important property to evaluate the effect of interactions between cell-material interfaces and it is the first step of cellular uptake process. Fibroblasts cells (NIH-3T3) were seeded in the presence and absence (control) of LDH and cell adhesion behavior was monitored after 24 h of incubation. **Figure 5.5a** exhibits that LDH has excellent cell adhesion property which also indicate the biofriendly nature of the material. **Figure 5.5b** demonstrates that LDH treated cells have elongated, well-spread healthy morphology with strong cell to cell contacts. This is to mention that the control cells also have healthy, elongated, well-spread morphology. Again, the biocompatibity of the developed LDH material has been accessed by using fibroblast cells (NIH 3T3) through MTT (3-(4,5-dimethylthiazol-2-yl)-2,5-diphenyltetrazolium bromide) assay technique as a function of both LDH concentrations and incubation time. As shown in **Figure 5.5c**, no apparent decrease in cell viability is noticed even though the LDH concentration reached as high as 300 μg ml^{-1}, revealing the excellent biocompatibility and nontoxicity of LDH. Again, the time dependent cell viability study (taking 30 μg/mL as working concentration) exhibits increased percentage of cell viabilities with increasing incubation time **(Figure 5.5d)**. The biocompatibity of the developed LDH material is also confirmed through fluorescence imaging by using 3T3cells after staining with acridine orange and ethidium bromide as a function of incubation time (1, 2, and 3 days). Consistent with the MTT assay measurement, **Figure 5.5e** also confirms healthy growing cells. These results therefore clearly suggest that the LDH possesses excellent cytocompatibility.

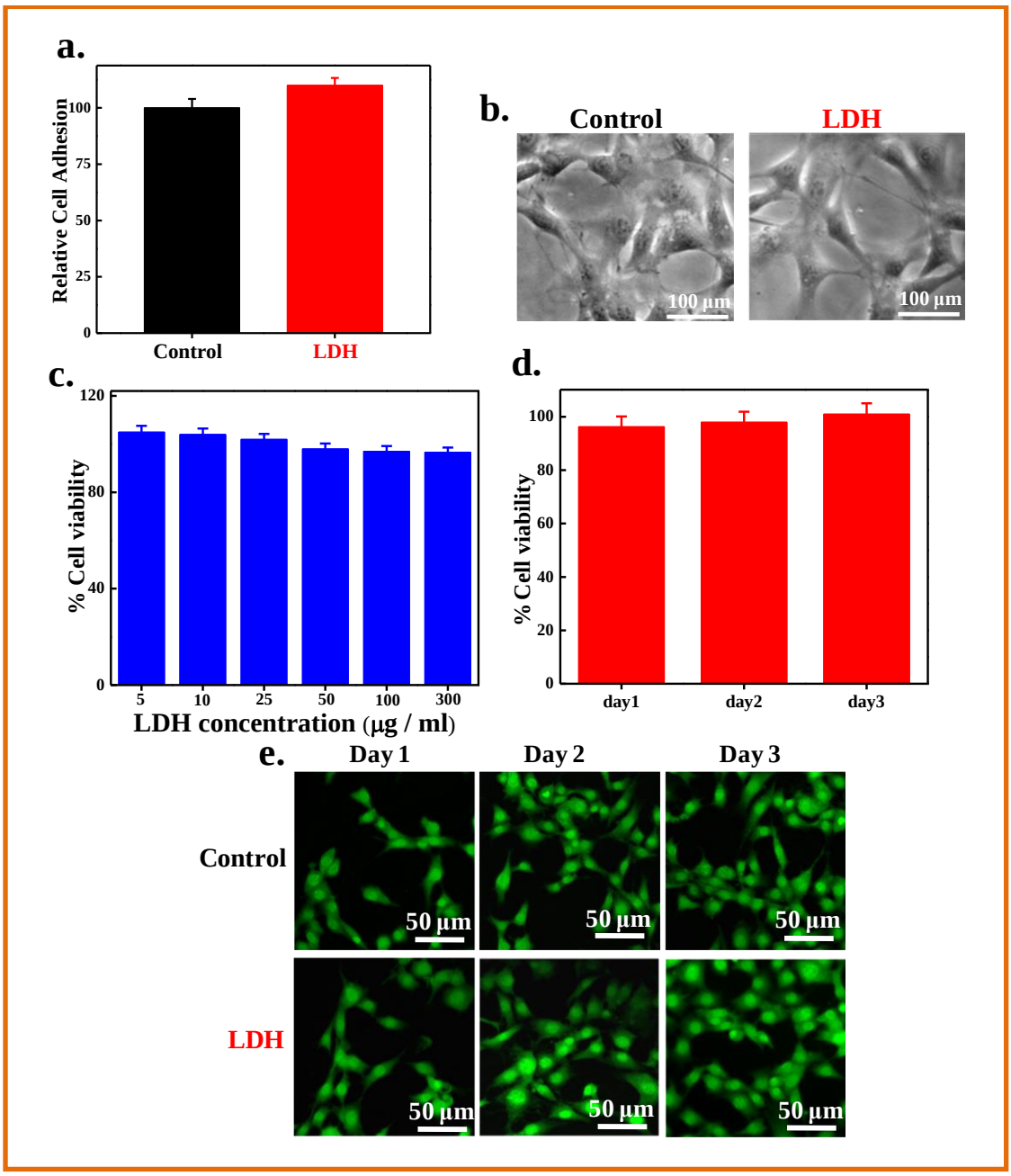

Figure 5.5: *In vitro* biocompatibility analysis; **(a)** Relative cell adhesion of LDH compared to control after 12 h incubation; **(b)** Phase contrast images of the NIH-3T3 cells grown on top of the LDH substrates after 12 h incubation; **(c)** Comparative cell viability study of LDH against NIH-3T3 cells using MTT assay as a function of concentration and **(d)** incubation time; Untreated cells are considered as control. The results are presented with mean ± standard deviation (SD) values obtained from three independent experiments; **(e)** Fluorescent microscopic images of NIH-3T3 cells after staining with AO/ EtBr dye.

5.2.6 Internalization of LDH into mammalian cell

The cell membrane permeability and internalization kinetics of LDH nanoparticles labeled with rhodamine B were examined to validate its efficiency as a gene delivery carrier into mammalian cells. As shown in **Figure 5.6a**, LDH shows rapid initial uptake

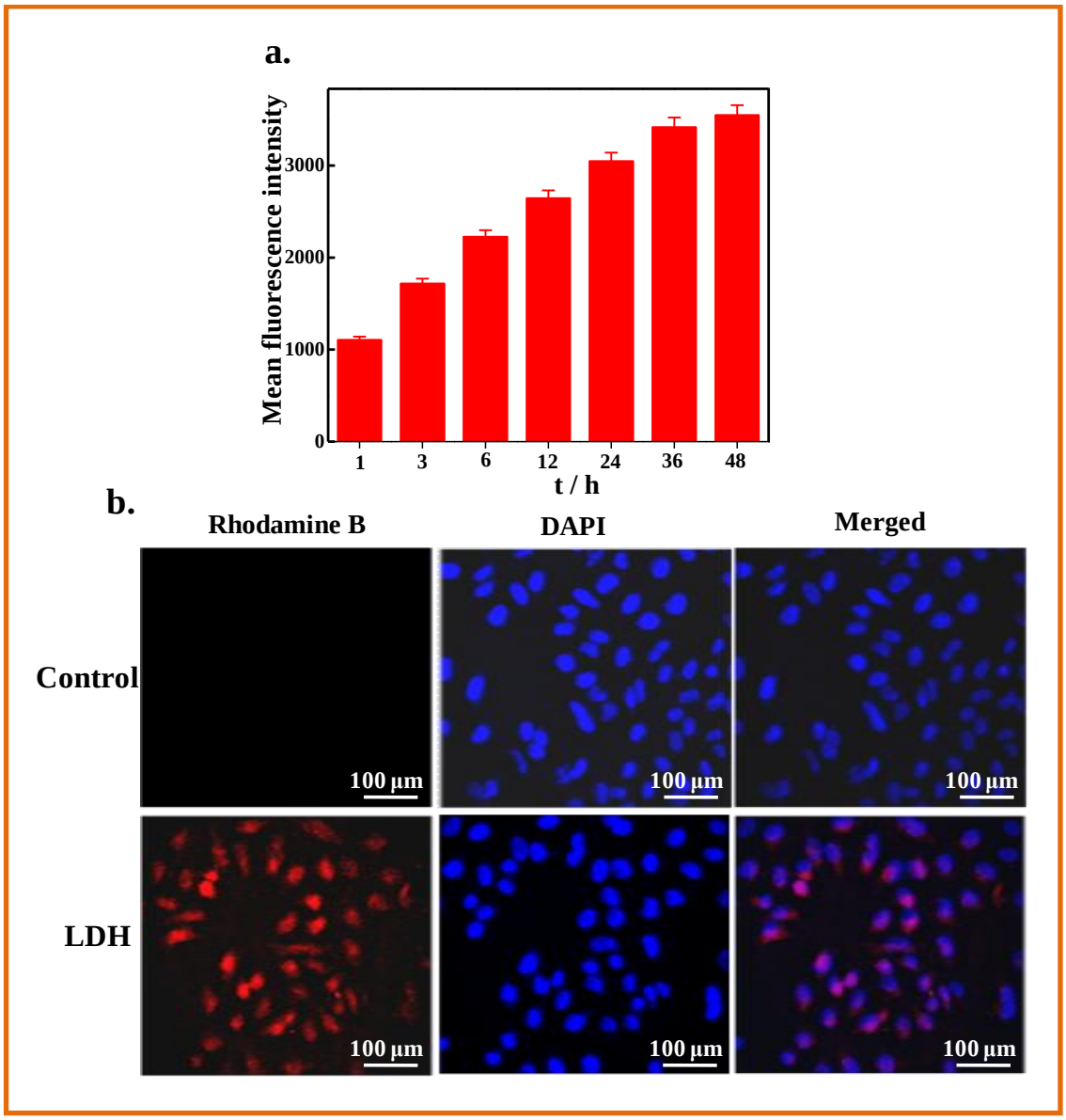

Figure 5.6: Cellular uptake kinetics of LDH nanoparticles into HeLa cells. **(a)** The observed rhodamine-B (RdB) fluorescence extracted from the cells in the presence of 100 µg ml^{-1} LDH- RdB. The results are presented in mean ± standard deviation (SD) values obtained from three independent experiments; **(b)** Fluorescence microscopic images showing the cellular uptake of rhodamine-B labeled LDH nanoprticles into HeLa cells.

up to 12 h incubation and then increases at a slower rate. The fluorescence micrograph also indicates that rhodamine B-labeled LDH (red fluorescence) is entered into HeLa cells and accumulated at nuclei and around the perinuclear region of the cytoplasm (**Figure 5.6b**). Nuclei are stained with DAPI, exhibiting blue fluorescence. These results therefore confirmed that LDH nanoparticles readily entered into cells across cell membranes without further supplementary materials such as cationic polymers and lipids.

5.2.7 pGFP transfection efficacy of LDH

Gene transfection experiment has been performed using pGFP-N1 DNA (0.5 µg, 4.7 kb) plasmid, a plasmid encoding green fluorescent protein. **Figure 5.7** demonstrates the fluorescence images of HeLa cells transfected with pGFP loaded to LDH nanocarrier. After 48 h of incubation in serum-containing media, bright green fluorescent over entire region of cells has been observed through the expression of GFP with LDH carrier. However, there is no expression of GFP with naked DNA observed.). The result therefore indicates that LDH has the potential to deliver pGFP into the cells efficiently.

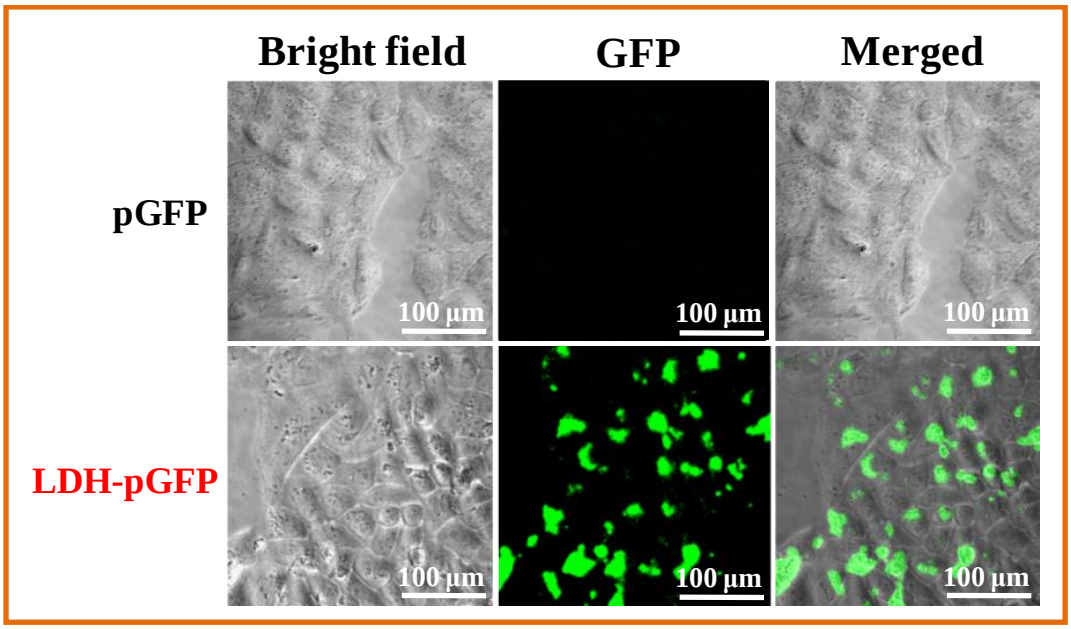

Figure 5.7: Fluorescence microscopy images of GPF expressing in HeLa cells. The images were captured at 48 h after the addition of samples.

5.2.8 Apoptosis in mammalian cancer cells mediated by GFP-p53:

Fluorescence microscopy is used to study GFP-p53 mediated apoptosis in HeLa cells after staining with acridine orange (AO) and ethidium bromide (EtBr). Cellular apoptosis, a biochemical event, is characterized by membrane blebbing, cell shrinkage, and fragmentation of the nuclear DNA. AO/EtBr double staining can easily distinguish the apoptotic cells from normal cells based on the permeability of cell membrane. Being cell-permeable, AO binds with DNA showing green fluorescence while EtBr is selectively taken up by apoptotic cells and stained the condensed nuclei with red fluorescence. **Figure 5.8** demonstrates that majority of cells exhibit green florescence in naked GFP-p53 even at higher concentration, while diffused or orange colored nuclei are observed in LDH–(GFP-p53) treated cells. The cells treated with 30 µg/ml LDH–(GFP-p53) exhibits orange and orange-red fluorescence, indicating membrane disruption. Hence, the developed LDH system has the potential to induce apoptosis in mammalian cancer cell mediated by GFP-p53 plasmid.

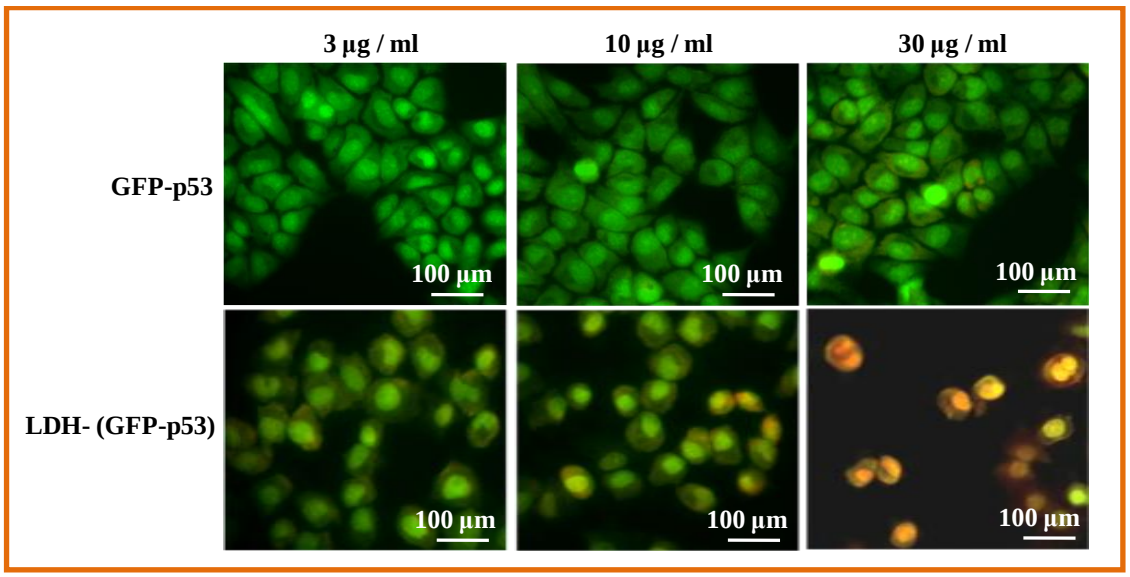

Figure 5.8: HeLa cells were stained with acridine orange/ethidium bromide after incubation with naked GFP-P53 and LDH-(GFP-P53) complex. Viable cells show green fluorescence. Apoptotic cells show orange and yellow fluorescence. Cells were observed under fluorescence microscope (x400).

5.3 Conclusion

Li-Al based LDH nanocarrier has been synthesized using coprecipitation method as a gene delivery vehicle. The developed LDH demonstrates high loading capacity of DNA and releases the loaded DNA in a controlled manner. The nanocarrier provides remarkable protection against DNase I and also can protect the vector from thermal damage. This vehicle also demonstrated excellent cellular uptake performances. Successful gene transfection has been achieved by using the developed LDH based nanocarrier. It is also found that the developed Li-Al LDH has efficiently induced GFP-p53 mediated apoptosis in HeLa cells to prove its efficacy.